Society For Biomaterials

Synthesis of nanostructured porous silica coatings on titanium and their cell adhesive and osteogenic differentiation properties

Débora Inzunza,[1] Cristian Covarrubias,[1] Alfredo Von Marttens,[2] Yerko Leighton,[2] Juan Carlos Carvajal,[2] Francisco Valenzuela,[1] Mario Díaz-Dosque,[1] Nicolás Méndez,[3] Constanza Martínez,[4] Ana María Pino,[3] Juan Pablo Rodríguez,[3] Mónica Cáceres,[4] Patricio Smith[4]

[1]Departamento de Ciencias Básicas, Laboratorio de Nanobiomateriales, Facultad de Odontología, Universidad de Chile, Sergio Livingstone 943, Independencia, Santiago, Chile
[2]Departamento de Prótesis, Facultad de Odontología, Universidad de Chile, Chile
[3]Laboratorio de Biología Celular, INTA, Universidad de Chile, Chile
[4]Facultad de Medicina, Pontificia Universidad Católica de Chile, Santiago, Chile

Received 10 October 2012; revised 18 January 2013; accepted 7 February 2013
Published online 9 April 2013 in Wiley Online Library (wileyonlinelibrary.com). DOI: 10.1002/jbm.a.34673

Abstract: Nanostructured porous silica coatings were synthesized on titanium by the combined sol–gel and evaporation-induced self-assembly process. The silica-coating structures were characterized by X-ray diffraction, transmission electron microscopy, scanning electron microscopy, and nitrogen sorptometry. The effect of the nanoporous surface on apatite formation in simulated body fluid, protein adsorption, osteoblast cell adhesion behavior, and osteogenic differentiation of human bone marrow mesenchymal stem cells (hBMSCs) is reported. Silica coatings with highly ordered sub-10 nm porosity accelerate early osteoblast adhesive response, a favorable cell response that is attributed to an indirect effect due to the high protein adsorption observed on the large-specific surface area of the nanoporous coating but is also probably due to direct mechanical stimulus from the nanostructured topography. The nanoporous silica coatings, particularly those doped with calcium and phosphate, also promote the osteogenic differentiation of hBMSCs with spontaneous mineral nodule formation in basal conditions. The bioactive surface properties exhibited by the nanostructured porous silica coatings make these materials a promising alternative to improve the osseointegration properties of titanium dental implants and could have future impact on the nanoscale design of implant surfaces. © 2013 Wiley Periodicals, Inc. J Biomed Mater Res Part A: 102A: 37–48, 2014.

Key Words: titanium, nanotopography, cell adhesion, osseointegration, sol–gel technique

How to cite this article: Inzunza D, Covarrubias C, Marttens AV, Leighton Y, Carvajal JC, Valenzuela F, Díaz-Dosque M, Méndez N, Martínez C, Pino AM, Rodríguez JP, Cáceres M, Smith P. 2014. Synthesis of nanostructured porous silica coatings on titanium and their cell adhesive and osteogenic differentiation properties. J Biomed Mater Res Part A 2014:102A:37–48.

INTRODUCTION

Titanium implants are used widely in the dental, maxillofacial, and ear–nose–throat fields as well as in orthopedic surgery. The ultimate goal of a prosthetic-implantological treatment is to obtain a life-long secure anchoring of the implant in the native surrounding bone. The success and lifetime of dental implants are largely dependent on the degree of osseointegration at the metal–bone interface.[1] Numerous studies have shown that the early events of bone healing around implants are related to their long-term clinical success.[2,3] Titanium and its alloys are the most commonly used load bearing implant materials, as these metals possess excellent mechanical properties, biocompatibility, and corrosion resistance. Still, titanium does not possess the capacity to establish the formation of a tight chemical bond with bone tissue. It is well known that the surface roughness of implants affects the rate of osseointegration and biomechanical fixation.[4] Microroughness (1–10 μm) maximizes the interlocking between mineralized bone and implant surface.[5,6] The suggestion that micrometer level surface topography results in greater accrual of bone at the implant surface is supported by some clinical evidence.[7,8] However, microrough surfaces have been generally interpreted as biocompatible with limited ability to directly affect the initial fate of surrounding tissues, that is, the ability to enhance bone formation or to prevent bone resorption.[9] The use of nanotopographical modifications on the implant surface to induce intrinsic osteoinductive signaling of the surface-adherent cells is another approach of current interest. Existing data supporting the role of nanotopography suggest that critical steps in osseointegration can be modulated by nanoscale modification of the implant surface.[10–13] Such changes alter the implant's surface interaction with ions, proteins (i.e., adsorption, configuration, bioactivity, etc.) and cells.

Correspondence to: C. Covarrubias; e-mail: ccovarru@u.uchile.cl
Contract grant sponsor: CONICYT through the FONDECYT; contract grant number: 11100495

These interactions can favorably influence molecular and cellular activities and alter the process of osseointegration.

Several techniques and approaches are used currently to produce nanotopographic modifications of endosseous implants.[14] Some of these approaches involve physical methods of compaction of ceramic particles to yield surfaces with nanoscale grain boundaries,[15] chemical treatments,[16] sandblasting/acid etching,[17] optical lithography,[18] galvanostatic anodization,[19] crystal deposition,[20] and monolayers to expose functional end groups that have specific functions.[21] A limitation of some of these methods is that they are random processes, so it is hard to control the uniformity and distribution of nanostructures on the implant surfaces. The synergetic coupling between soft matter physical chemistry and inorganic or hybrid sol–gel chemistry has opened new possibilities for advanced control of nanoscale topography. These novel materials offer a high degree of versatility in terms of structure, texture, and functionality.[22] Self-assembly is a general phenomenon which is well known and is used in nanoscience to produce ordered structures using well-defined nano-objects.[23] In particular, colloids self-organize into ordered layers during evaporation of the solvent; this process is commonly known as evaporation-induced self-assembly (EISA). Sol–gel processing coupled with the EISA technique opened the possibility of rapid production of patterned nanoporous materials in the form of films.[24,25] EISA involves nanotexturation via the liquid deposition of condensable inorganic precursors in the presence of micelle-forming surfactants.[26] Such a method is simple, cheap, scalable, and gives high reproducibility without expensive, specialized equipment. Nanoporous silica films prepared by the sol–gel/EISA technique were applied for the first time on a titanium surface by Gomez-Vega et al.[27] This silica coating exhibited the capacity to form apatite when soaked in simulated body fluid (SBF), and this is attributed to the nanoporous structure and to the presence of abundant silanol groups. However, no further studies have been reported to confirm the effect of the nanopores on apatite formation by comparison with appropriate control surfaces. In addition, it has not been reported whether these highly ordered nanoporous structures can affect the adhesive and osteogenic behavior of bone-forming cells. Some studies show that topographic features, such as pillars, islands, or pits with an interfeature or *z*-scale dimension greater than 50–60 nm impair focal adhesion and cell response.[28–31] Conversely, decreasing the interfeature distance or *z*-dimension below 50 nm or increasing it to the microscale facilitates stem-cell adhesion and functional differentiation.[32,33] However, there is insufficient information about the effect of uniformly nanometer-sized pores smaller than 10 nm, and how these nanostructures with unique surface properties can influence extracellular protein adsorption and consequently cell behavior.

In the present work, highly ordered nanoporous silica coatings were synthesized on titanium surfaces by the sol–gel/EISA technique. The effect of the sub-10 nm nanostructured porosity of the silica coatings on apatite formation in SBF, protein adsorption, osteoblast cell adhesion behavior, and osteogenic differentiation of human bone marrow mesenchymal stem cells (hBMSCs) is reported.

MATERIALS AND METHODS

Synthesis of silica coatings on a titanium surface

Silica coatings were prepared on sheets of Ti6Al4V titanium alloy (Zimmer Dental) using the EISA sol–gel technique. Titanium sheets (15 mm $\times$ 15 mm $\times$ 1 mm) were sanded with silicon carbide paper (800 grit) and cleaned ultrasonically with acetone and ethanol before use. The coating sol solutions were prepared using both the amphiphilic triblock copolymer Pluronic P123 (P123; EO20PO70EO20, Mw = 5800; Aldrich) and poly(ethylene glycol) (Mw = 600, PEG) as pore structure-directing agents (SDAs). Briefly, 3.7 g of tetraethyl orthosilicate (98%; Aldrich) were prehydrolyzed in a solution containing 20 mL of ethanol (95%) acidified with 0.5 mL of HCl 0.5 *N* (pH 2.0) under vigorous stirring at room temperature for 20 min. This prehydrolyzed silica solution was added to a solution containing 2 g of the SDA dissolved in 20 mL of ethanol. The resulting solution was then submitted to an aging period at room temperature for 24 h with stirring, and films were prepared by slip coating on the titanium sheets. Essentially nonporous silica (NPS) coatings were prepared as control, using the same procedure described above, but without the addition of SDA to the ethanol solvent.

Silica coatings doped with calcium and phosphate ions were also prepared. The calcium and phosphate content in the silica coating was chosen using the composition of mesoporous bioactive glasses as reference.[34] For this purpose, 0.34 g of triethylphosphate (Aldrich, 99.8%) and 0.49 g of $Ca(NO_3)_2{\cdot}3H_2O$ (Sigma-Aldrich) were dissolved in the prehydrolyzed silica solution, and the procedure described above was followed.

For the slip-coating procedure,[35] the titanium sheet was suspended in an inverted position with a pair of tweezers attached to a clamp fixed loosely enough to a stand to allow rotation of the tweezers. The polished side was brought in contact with the silica sol. The titanium sheet was kept in this half-immersed position for 20 s, slipped away horizontally by rotating the tweezers, and then dried in a vertical position for 40 s. The silica coatings were kept for 24 h at 35°C, and then calcined by heating at a rate of 0.5°C/min to 400°C, holding that temperature for 4 h to remove the SDA.

Characterization of the silica coatings

The unmodified and silica-coated titanium surfaces were examined by scanning electron microscopy (SEM; Zeiss, DMS 940) after coating the surfaces with gold. The structural order of the porous silica coatings was analyzed by low-angle X-ray diffraction (XRD) within a 2θ range of 0.5–5°. XRD patterns were collected on a Siemens D 5000 diffractometer using CuKα radiation at a scanning speed of 0.2°/min. The porous nanostructure was examined by high-resolution transmission electron microscopy on a FEI-Tecnai G2 F20 S-Twin high-resolution transmission electron microscope equipped with a field emission gun operating at an accelerating voltage of 120 kV. Plan-view film specimens

were prepared by removing the silica films from a titanium sheet and suspending them in ethanol. This suspension was then dispersed on a holey carbon film supported by a copper grid. Textural characterization of silica films was carried out by N_2 adsorption at 77 K in a Micromeritics ASAP 2010 sorptometer. The specific apparent surface areas (S_g) were calculated using the Brunauer–Emmett–Teller equation, and the micropore volume (V_o) by the Dubinin–Radushkevich equation applied to the experimental data obtained from N_2 adsorption isotherms. Pore diameter was estimated from the pore size distribution curves obtained by the Barrett–Joyner–Halenda method.

In vitro bioactivity assays

The ability of the silica coatings to induce the formation of apatite was assessed in acellular SBF, which has inorganic ion concentrations similar to those of human extracellular fluid. The SBF solution was prepared according to the procedure described elsewhere[36] using the standard ion composition (Na^+ 142.0 m*M*, K^+ 5.0 m*M*, Mg^{2+} 1.5 m*M*, Ca^{2+} 2.5 m*M*, Cl^- 147.8 m*M*, HCO_3^- 4.2 m*M*, HPO_4^{2-} 1.0 m*M*, and SO_4^{2-} 0.5 m*M*). The fluid was buffered at physiological pH 7.4 at 37°C with tri-(hydroxymethyl) aminomethane and hydrochloric acid. The unmodified and silica-coated titanium sheets (1.5 cm^2) were individually soaked in 20 mL of SBF in polyethylene containers at 36.5°C using a thermostatic bath. After incubation for a designated time period, the samples were removed from the SBF, rinsed with distilled water, and dried at 60°C. Apatite mineralization on the surfaces was also analyzed by SEM with a Jeol JSM 5410 microscope equipped with energy-dispersive X-ray spectroscopy (EDX).

Cell culture

Human osteoblastic osteosarcoma cell line (SaOS-2) was used to evaluate cell adhesion and morphology on the silica-coated titanium surfaces. Approximately 50 $\times$ 10^3 cells in 1 mL of Dulbecco's modified Eagle medium (DMEM; Invitrogen Life Technologies) were seeded on the titanium sheets (10 mm $\times$ 10 mm). The medium contained 10% fetal bovine serum (FBS GIBCO), 50 IU/mL penicillin, and 50 mg/mL streptomycin. The cell suspension was seeded on sterilized titanium samples and incubated at 37°C in a humidified air atmosphere containing 5% CO_2. Cells that adhered on the surfaces after 2 h of incubation were examined by SEM. For this purpose, adherent cells were fixed in 2.5% glutaraldehyde, then progressively dehydrated in ethanol, dried in supercritical CO_2, and finally coated with gold for SEM observation. The viability of the osteoblast-like cells on the surfaces was evaluated using the 3-(4,5-dimethylthiazol-2-yl)5-(3-carboxymethoxyphenyl)-2-(4-sulfophenyl)-2H-tetrazolium (MTS) assay according to the protocol provided by the manufacturer (CellTiter Aqueous One Solution cell proliferation assay kit from Promega). MTS assays were performed in quadruplicate after 2, 7, 9, and 14 days of cell culture. Briefly, after 2 h of incubation with the MTS reagent in a humidified 5% CO_2 atmosphere, the medium was

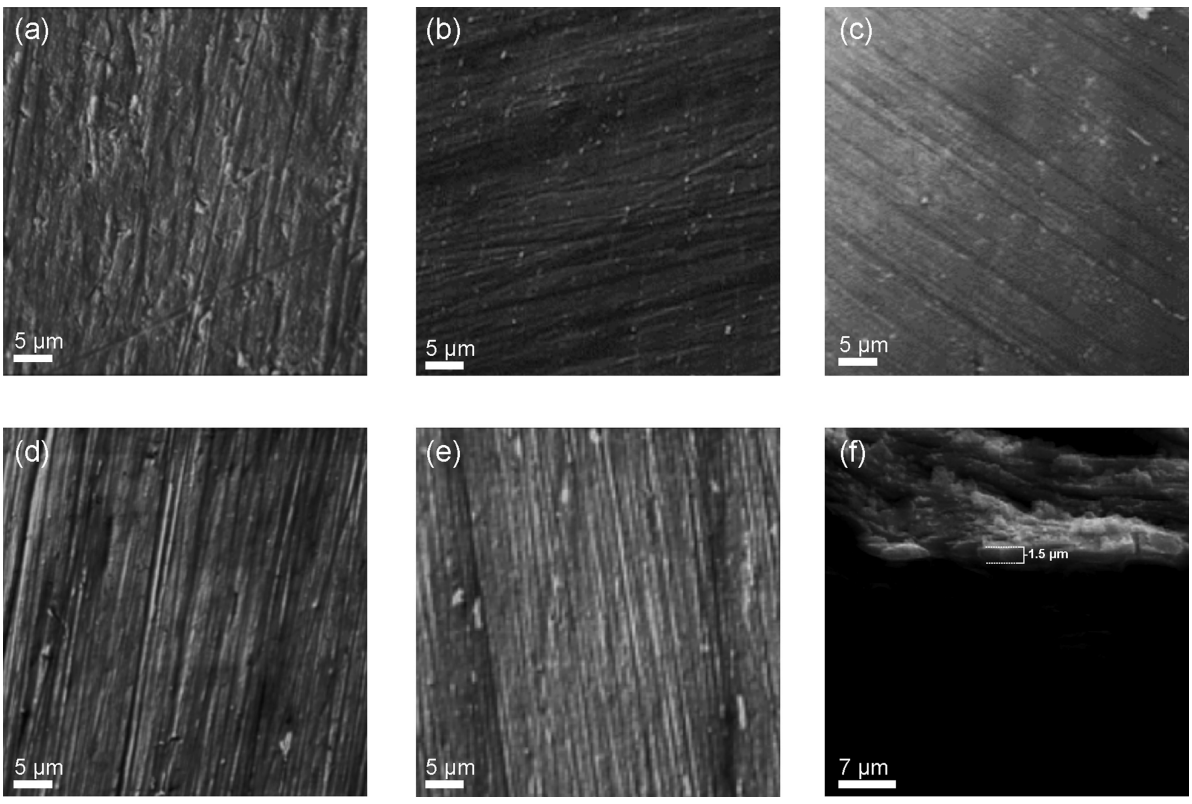

FIGURE 1. Scanning electron microscopic images of (a) unmodified titanium surface, and coated surfaces with (b) NPS, (c) PEG, (d) P123, and (e) CaP-P123 films. (f) Cross-section of P123-coated titanium surface.

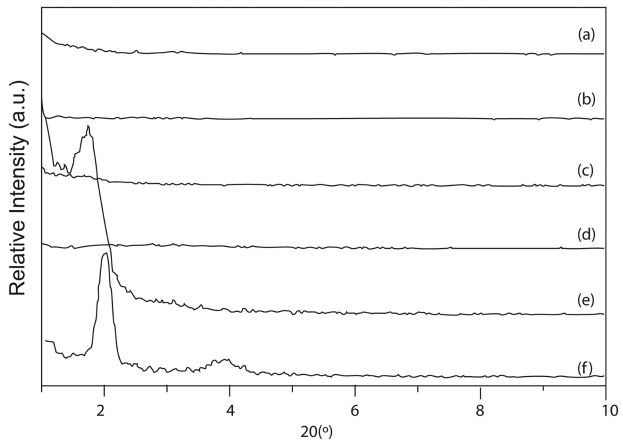

FIGURE 2. XRD pattern of (a) CaP-NPS, (b) NPS, (c) CaP-PEG, (d) PEG, (e) CaP-P123, and (f) P123 coatings.

collected from the samples and absorbance was measured at a wavelength of 490 nm using an ELISA microplate reader (Tecan Infinite F-50).

The osteogenic differentiation of hBMSCs on the titanium surfaces was also evaluated. hBMSCs, $1 \times 10^3/cm^2$, were seeded on the titanium surfaces and maintained in basal culture medium (DMEM supplemented with 10% FBS, 100 IU/mL penicillin, and 100 μg/mL streptomycin). The medium was changed every 3–4 days. After 10 days of culture, mineralized nodule formation on the titanium surfaces was examined by SEM and nodule composition analyzed by EDX. Cells were also examined by epifluorescence microscopy. For this purpose, adherent cells were fixed in *p*-formaldehyde 4%–ethanol 9:1 for 30 s. Cell nuclei were stained with Hoeschst 33342 0.2 μg/mL for 10 min. Images were captured using a Niko Eclipse 50i Epi-Fluorescence Microscope.

Alkaline phosphatase (ALP) activity was measured after different times of cell culture, cells grown on the titanium surfaces were fixed with 90% ethanol and 10% formaldehyde (37%) during 1 min, and then washed with PBS. The fixed cells were incubated with 5 μ*M* *p*-nitrophenol phosphate (Sigma) during 20 min at 37°C, and the *p*-nitrophenol generated was quantified by reading the absorbance at 405 nm on an ELISA microplate reader (Tecan Infinite F-50).

Protein adsorption

Bovine serum albumin (Merck) and human plasma fibrinogen (Merck) were used as model proteins. Solutions containing 0.4 mg/mL of protein were prepared in a pH 7.4 phosphate buffer (K_2HPO_4/KH_2PO_4 100 m*M*), and 1.5 mL of protein solution was contacted with the titanium surface ($10 \times 10 \times 1$ mm) in a 24-well cell culture plate, and then incubated at 37°C for 6 h. The surfaces were then washed with phosphate buffer to remove the nonadherent proteins. Each sample was transferred to a 20 mL glass vial containing 1.5 mL of 2% sodium dodecyl sulfate solution, and subsequently incubated at 37°C in a thermostatic bath for 12 h to extract adhered proteins. Protein concentration was

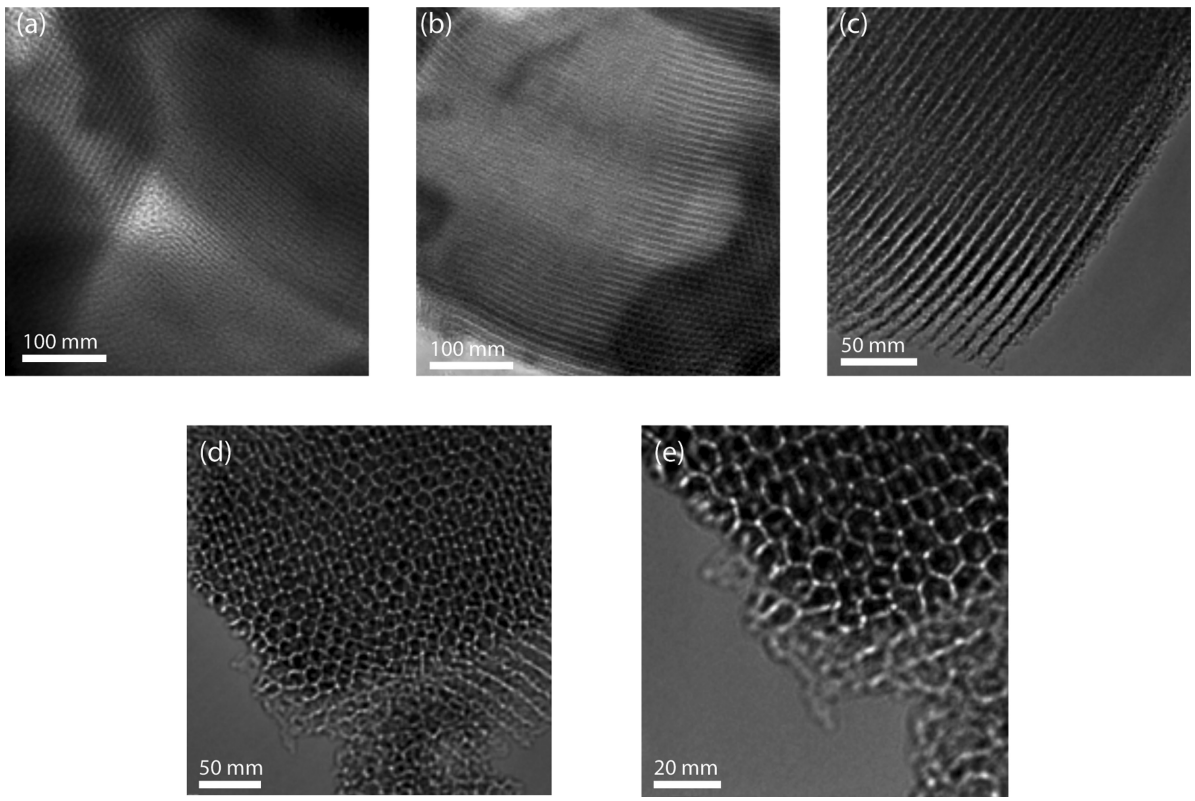

FIGURE 3. HRTEM images showing the highly ordered nanoporous structures of (a) P123 and (b and c) CaP-P123 coatings.

TABLE I. Textural Properties of Porous Silica Coatings

	S_g (m^2/g)	d_p (nm)	V_p (cm^3/g)	V_o (cm^3/g)	V_m (cm^3/g)
NPS	1.7	–	–	–	–
CaP-NPS	0.4	–	–	–	–
P123	423	3.8	0.42	0.18	0.24
CaP-P123	411	4.7	0.5	0.18	0.38
PEG	467	2.3	0.19	0.19	0.00
CaP-PEG	688	2.3	0.32	0.30	0.27

S_g, specific surface area; d_p, pore diameter; V_p, total pore volume; V_o, micropore volume; V_m, mesopore volume.

determined using the spectrophotometric Micro Bicinchoninic Acid Assay Kit (Thermo Scientific) according to the manufacturer's instructions.

RESULTS AND DISCUSSION

Preparation of silica coatings

Silica coatings using P123 and PEG as pore SDAs were synthetized on the titanium surfaces. In addition, an essentially NPS coating and the corresponding calcium- and phosphate-doped coatings (CaP) were also prepared. Scanning electron microscopic images (Fig. 1) taken on the different surfaces show that uniform silica films were obtained on the metal surface. In all cases, the silica layers were smooth and did not exhibit microdefects. The thickness of the silica films estimated from the SEM cross-section was about 1.5 μm [Fig. 1(f)]. The nanostructural order of the silica coatings was analyzed by XRD (Fig. 2). The XRD patterns of the P123 film present the characteristic reflections corresponding to a highly ordered hexagonal mesoporous silica

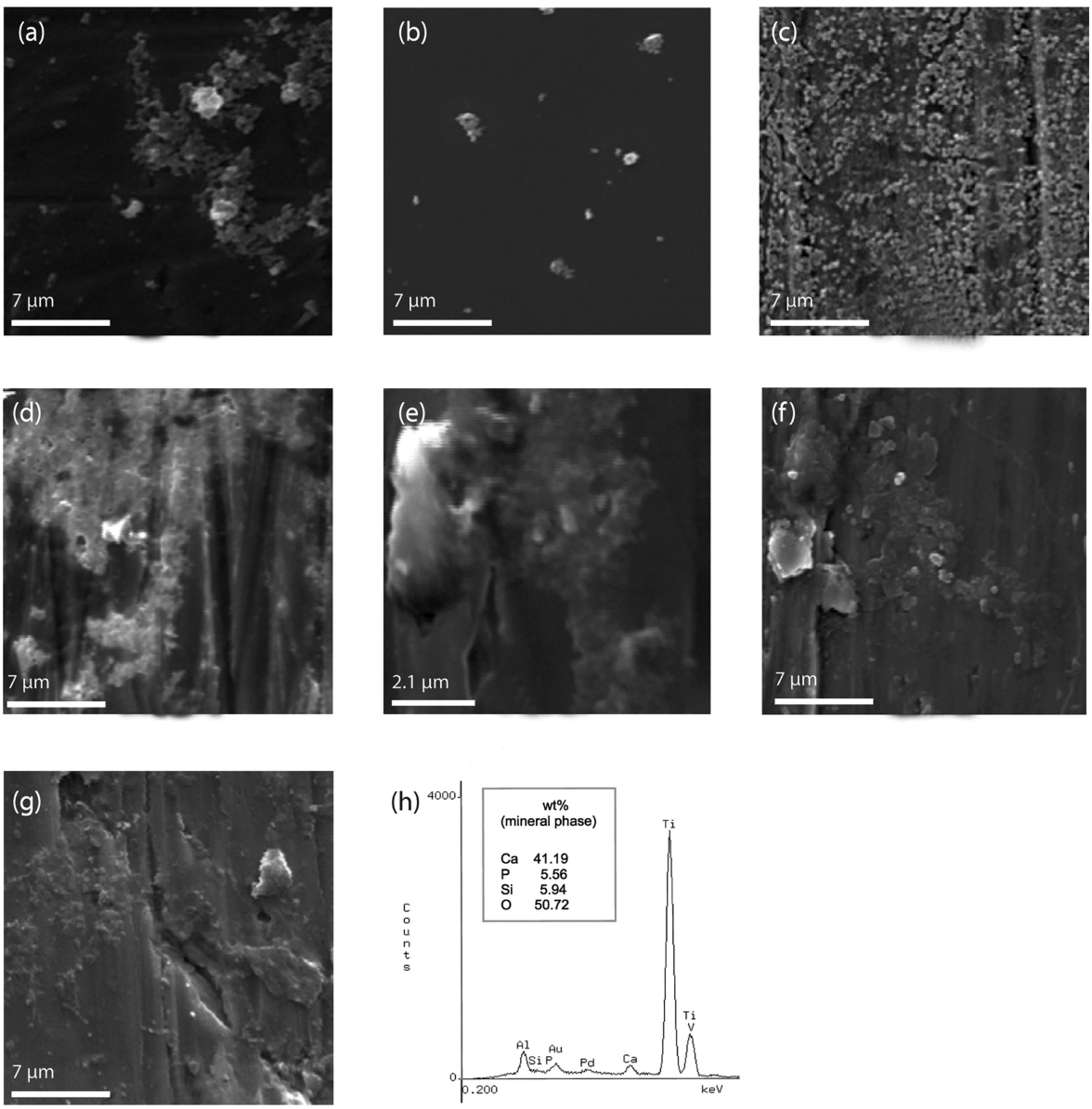

FIGURE 4. Scanning electron microscopic images of titanium surfaces after 7 days of immersion in SBF: (a) unmodified titanium, (b) NPS, (c) CaP-NPS, (d) P123, (e) CaP-P123, (f) PEG, and (g) CaP-P123 after 30 days of immersion in SBF. (h) EDX elemental analysis of CaP-P123 surface after 7 days of immersion in SBF.

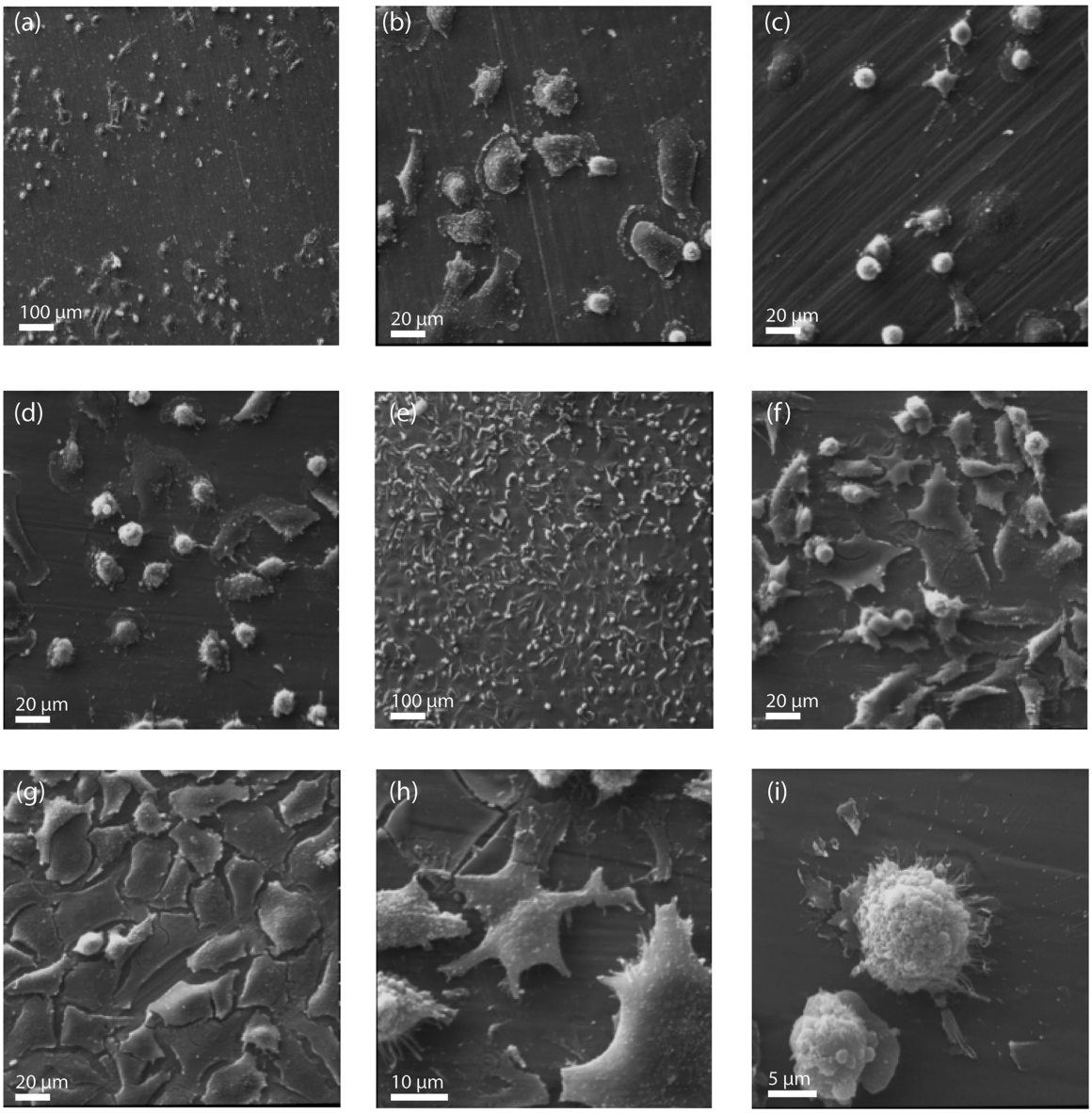

FIGURE 5. Scanning electron microscopic images of human osteoblast-like SaOS-2 cells adhered on titanium surfaces after 2 h of incubation: (a and b) unmodified titanium, (c) NPS, (d) PEG, (e and f) P123, and (g) CaP-P123. High magnification showing the morphology of cells adhered on (h) P123 and (i) NPS surfaces.

structure,[37] while PEG and NPS coatings exhibit no structural order. The incorporation of calcium and phosphate in the P123 silica film (CaP-P123) produced a cubic porous silica structure,[38] as judged by the reflection from the (110) plane at a 2θ value of 1.8°. High-resolution transmission electron microscopic (HRTEM) images (Fig. 3) show that these self-ordered films consist of an array of uniform nanopore channels. Although the pore channels are preferentially oriented parallel to the titanium surface, pore channels aligned perpendicular to the substrate can be also observed, particularly on the CaP-P123 film. The diameter of these cylindrical pore channels estimated from HRTEM images is around 4 nm. Textural characterization results of the silica coatings (Table I) show that the ordered P123 silica coatings have a specific surface area around 400 m^2/g, and pore diameter values of 3.8–4.7 nm, which match well those estimated through HRTEM images. Although the PEG silica coatings present no structural order, their surface area was as high as 467–688 m^2/g, which can be accounted for their smaller pore diameter (2.3 nm) and consequently larger micropore volume (0.19–0.30 cm^3/g). The surface area of the NPS coatings was very low and no porosity was detected, confirming their essentially nonporous structure.

In vitro bioactivity assays

For a preliminary evaluation of the bioactivity of the silica-coating surfaces, *in vitro* testing was performed in SBF. Scanning electron microscopic images reveal a low degree

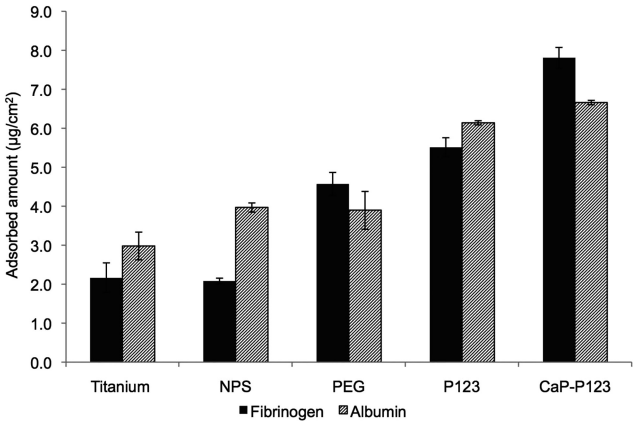

FIGURE 6. Protein adsorption on the unmodified titanium surface and on those coated with the nanostructured silica films after 6 h of incubation in a 0.4-mg/mL protein solution.

of mineralization on the unmodified titanium (Ti) as well as on the NPS-coated surface (Fig. 4). Although mineralization is increased with the incorporation of CaP in the NPS coating, only small discrete mineral crystals are formed. In contrast, a higher degree of mineralization in terms of density, extension and cluster mineral size can be seen on the surfaces coated with the nanoporous silica films (P123, PEG), which is increased with the incorporation of CaP [Fig. 4(f)] and notably after 30 days of incubation [Fig. 4(g)]. Although the mineral phase was not detected by XRD, EDX chemical analysis [Fig. 4(h)] shows that this mineral layer has an appreciable Ca and P content. This mineral layer may correspond to either an amorphous calcium–phosphate layer or to a crystalline apatite phase. The higher degree of mineralization presented by the nanoporous surfaces (P123, PEG) can be attributed to the large-specific surface area of these silica coatings. High-surface free energy as well as the concentration of surface silanol groups are factors known to favor the process of apatite nucleation and growth in SBF.[39] Also, the composition used in the preparation of the CaP-P123 coating should generate a mesoporous bioactive glass material[40] on the titanium surface, which has a proven ability to induce the formation of bone-like apatite in SBF.

Osteoblast cell adhesion

Although the SBF assay is a useful method for the preliminary evaluation of the potential bone-bonding ability of a biomaterial,[41] cell behavior studies generally provide a more realistic information about *in vivo* bioactivity. Cell adhesion behavior on the nanostructured surfaces was evaluated using SaOS-2 osteoblast-like cells. Scanning electron microscopic images of adherent cells (Fig. 5) show differences in cell density and morphology on the surfaces with different porous textures. The ordered nanoporous P123 surfaces [Fig. 5(e–h)] exhibited a density of adherent cells significantly higher than that found on the Ti, NPS, and PEG surfaces. Moreover, most of the osteoblast-like cells spread

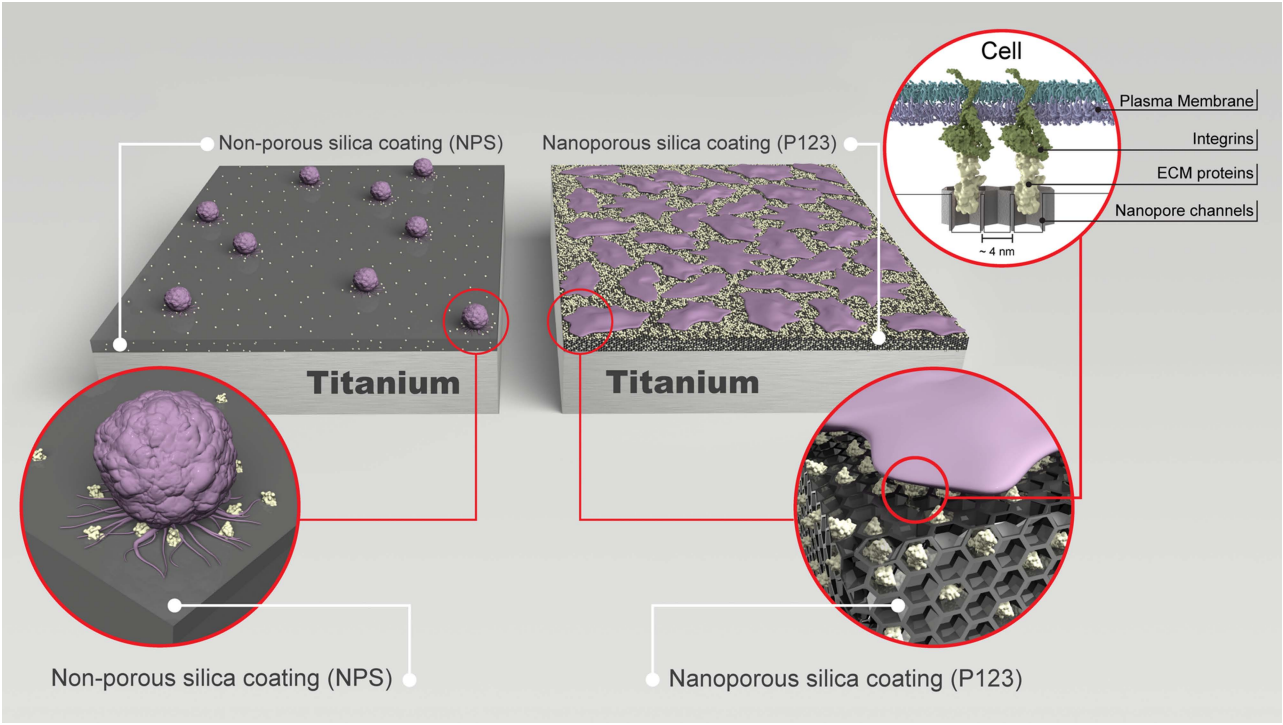

FIGURE 7. Schematic representation of the effect of highly ordered porous silica nanostructure on ECM protein adsorption and cell adhesion behavior. The absence of nanopores in the NPS surface decreases ECM protein adsorption and the amount of adhered cells, keeping the round shape of the cells in early attachment stages. The high-specific surface area of the hexagonal/cubic nanostructured porous P123 surface increases ECM protein adsorption and consequently the density of adherent cells. The nanoporous structure accelerates the cell attachment process toward the spreading and flattening stages. [Color figure can be viewed in the online issue, which is available at wileyonlinelibrary.com.]

well on the P123 surface, whereas cells adhered on the other surfaces were mostly round in shape. According to Rajaraman et al.,[42] cellular adhesion and spreading occur through four events: attachment, filopodial growth, cytoplasmic webbing (spreading), and flattening of the central mass. The duration of these phases and their degree of overlapping may vary between different substrates.[43] In the present study, the effect of nanoporous structures on cell adhesion behavior can be observed by comparing the lamellipodial morphology adopted by the cells on the P123 surface with the round shape exhibited on the NPS surface [Fig. 5(h,i)]. These observations indicate that the nanoporous P123 surface appears to accelerate the cell attachment process toward the final spreading and flattening stages. Also, cell adhesion is further increased on the CaP-P123 coating having a bioactive glass chemical composition. The high density of spreading cells on the P123-coated titanium surfaces can be attributed to the high-specific surface area and larger pore size of the P123 coatings. We hypothesize that high-specific surface area accessible through larger pore sizes increases the adsorption of extracellular matrix (ECM) proteins, which are known to mediate cell attachment and proliferation behavior.[44] In order to verify this effect, the adsorption of albumin and fibrinogen was studied on the different surfaces. Figure 6 shows the amount of adsorbed protein on the Ti- and silica-coated surfaces. It is seen that the protein adsorption capacity of the large-surface area ordered nanoporous coatings (P123, CaP-P123) is statistically higher than that of the other surfaces. Although the PEG coating also has a large surface area (Table I), the PEG structure has a smaller pore diameter (2.1 nm) which probably limits albumin (4 nm $\times$ 4 nm $\times$ 14 nm[45]) and fibrinogen (6.5 $\times$ 6.5 $\times$ 46 nm[46]) adsorption on the internal surface. In addition, the protein adsorption process should be favored on the highly ordered and uniform P123 nanoporous structure compared to that taking place on the irregular and discontinuous PEG porosity.[47] The relatively low protein adsorption capacity exhibited by the NPS surface shows that the presence of sub-10 nm porosity plays an important role in the protein adsorption process. These protein adsorption results agree well with the cell adhesion behavior exhibited by the surfaces, showing good correlation between the amount of adsorbed proteins and the density of adherent cells. It is well known that cells adhere to the substrate using integrin transmembrane complexes (focal adhesion) with variable specificity for ECM proteins.[48] Therefore, the concentration of ECM proteins on the implant surface largely affects adhesive cell behavior as schematized in Figure 7. The results of the current study show that the highly ordered nanoporous silica coating with high surface energy increases ECM protein adsorption and consequently accelerates the osteoblast's adhesive response on the titanium surface. Quantitative MTS assays were also performed to determine the metabolic activity of SaOS-2 cells cultured on each surface for different incubation times (Fig. 8). In general, no statistical differences were found between the absorbance values of the silica surfaces with those of Ti and the control (cells cultured in the absence of the materials), indicating that the viability and proliferation of the osteoblast-like cells is not altered in contact with the silica coatings prepared in this work.

hBMSC differentiation

Adhesion and spreading of cells on the implant surface are the initial phase for cellular function, and surface implant nanostructure may also affect the osteogenic differentiation of stem cells. In order to investigate the nanostructure-influenced cell differentiation effect, hBMSCs were cultured on the different surfaces. Figure 9 shows the SEM and epifluorescence images of the surfaces after 10 days of cell culture

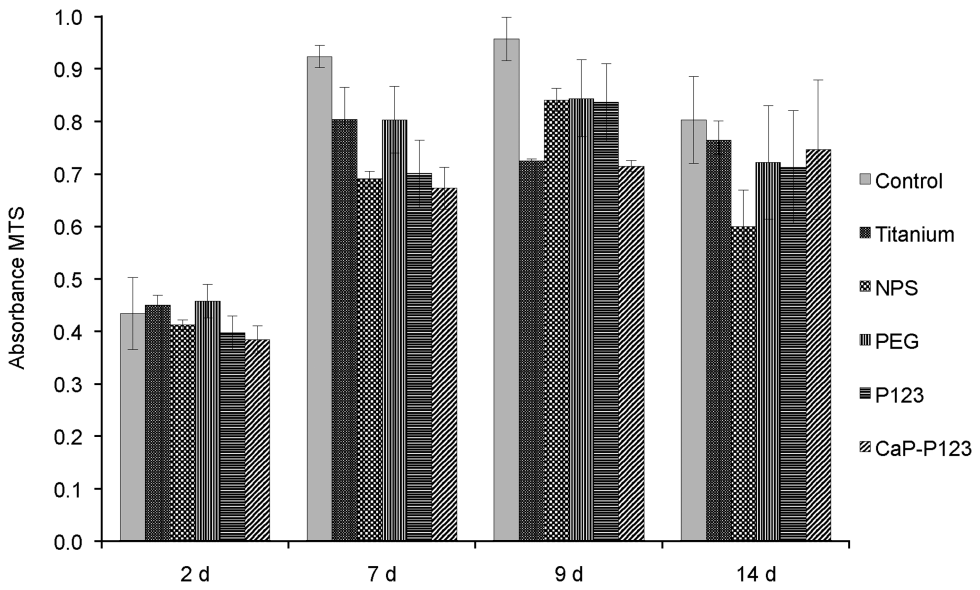

FIGURE 8. Human osteoblast-like SaOS-2 cell viability (MTS) on the unmodified titanium surface and on those coated with the nanostructured silica films at different culture times.

in the absence of osteogenic supplements. After this prolonged cell culture period, it can be seen that the hBMSCs covered the entire surfaces, forming a dense and continuous layer. Epifluorescence images show the cell nucleus, confirming the presence of cells in the smooth surface layer. Scanning electron microscopic images reveal the formation of an abundance of mineralized nodules associated with cells grown on the nanoporous silica-coated surfaces [Fig. 9(c–e)]. Particularly, numerous nodules were formed on the highly ordered P123 porous silica surfaces. It is interesting to note, however, that no nodule formation was detected in cultures on Ti control, and hardly any on the NPS surface [Fig. 9(a,b)]. EDX chemical composition analysis [Fig. 9(i)] shows that the mineralized nodules have high Ca and P

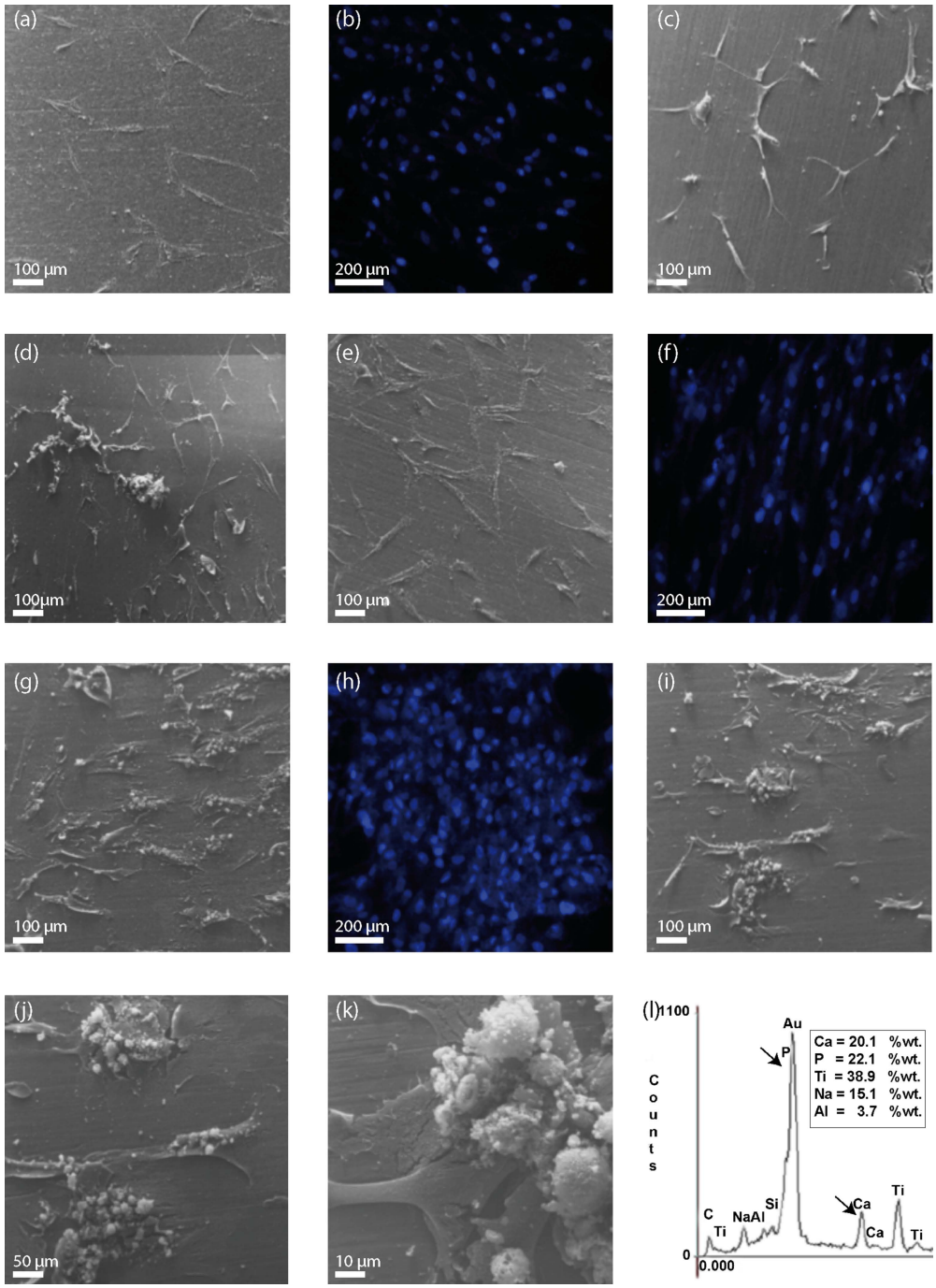

FIGURE 9. Scanning electron microscopic images of hBMSCs after 10 days of culture on titanium surfaces: (a) unmodified titanium—10 days, (c) NPS—10 days, (d) PEG—10 days, (e) P123—1 days, (g) P123—10 days, (i) CaP-P123—10 days. (j and k) High magnification showing hBMSCs associated with mineralized bone nodules on CaP-P123—10 days surface. Epifluorescence images showing the nuclei in the hBMSCs cultured on: (b) unmodified titanium, (f) P123—10 days, and (h) CaP-P123. (i) EDX elemental analysis of the mineralized nodule. [Color figure can be viewed in the online issue, which is available at wileyonlinelibrary.com.]

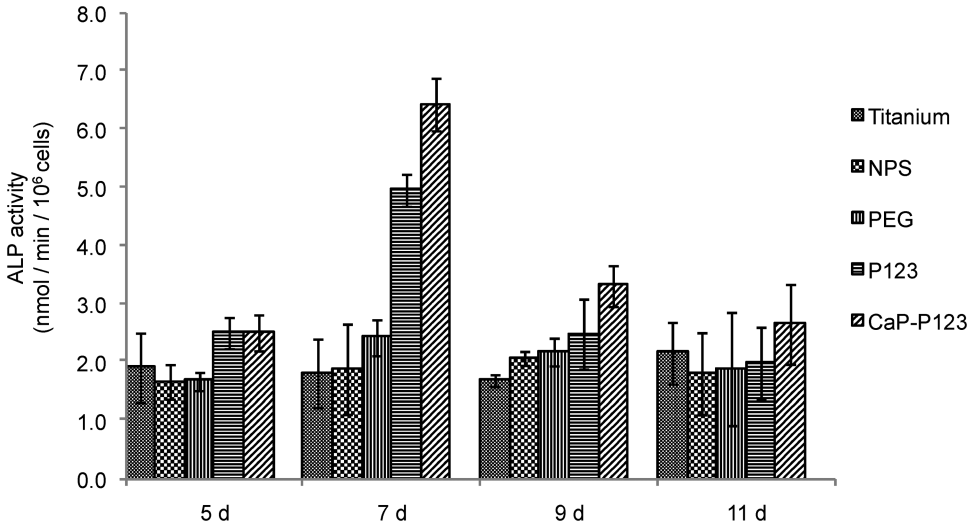

FIGURE 10. ALP activity of hBMSCs grown on the different surfaces tested in basal media at different culture times.

content, which may correspond to partially crystallized apatite deposits or mineralized matrix vesicles produced during the cell-mediated bone formation process.[49,50] These nodules were not observed after short-term (1 day) cultures [Fig. 9(d)] or by using an acellular culture medium as control. Our preliminary observations indicate that the nanostructured silica coatings promote the osteogenic differentiation of hBMSCs in the absence of osteogenic supplements. In addition, statistically significant higher ALP activity values were measured on the P123 and CaP-P123 nanoporous surfaces at 7 days of culture (Fig. 10), confirming the favorable effect of these surfaces on the osteogenic differentiation process. ALP activity is a differentiation marker that commonly decline after "extensive" mineralization,[51] which can be observed after prolonged culture times. Osteogenic differentiation of stem cells may be influenced through both ECM protein changes and direct cell interaction with the nanofeatured surface.[52,53] In the present study, porous silica nanostructure modifies ECM protein adhesion, but it can also directly affect the stem cell differentiation process. Increasing evidence indicates that mechanical signals from nanostructured surfaces may be transmitted via integrins through the cytoskeleton to the nucleus, affecting the expression of bone-related transcription factors.[54,55] In addition, bioactive glass-type CaP-P123 coating, through its ionic dissolution products, can chemically drive hBMSCs along the osteoblastic pathway,[56,57] resulting in increased mineralizing activity. The results of the present work show that silica coating with highly ordered sub-10 nm porous structure induces an enhanced osteogenic cell response, which could promote faster and more reliable osseointegration of titanium implants.

CONCLUSIONS

The sol–gel/EISA technique allows the preparation of uniform silica coatings with highly ordered hexagonal/cubic porous nanostructure on titanium surfaces. The nanoporous silica surface accelerates early osteoblast adhesive response, which is attributed to the high ECM protein adsorption on its large-specific surface area, but also probably to direct mechanical stimulus from the sub-10 nm topography. The nanoporous silica surface, particularly that doped with calcium and phosphate, also promotes the osteogenic differentiation of hBMSCs with spontaneous mineral nodule formation in basal conditions. The bioactive properties exhibited by the nanostructured porous silica coatings may be used to improve the osseointegration of titanium implants and have future impact on the nanoscale design of implant surfaces.

ACKNOWLEDGMENTS

The Vicerrectoria de Investigación y Desarrollo (VID)—Universidad de Chile is also grateful for the Faculty Travel Grant Program "U-Apoya: Línea Ayuda de Viaje." We also wish to thank Prof. Nancy Olea (CESAT-ICBM, University of Chile) for her assistance in SEM specimen preparation and imaging of cell samples.

REFERENCES

1. Hedia HS, Mahmoud NA. Design optimization of functionally graded dental implant. Biomed Mater Eng 2005;14:133–143.
2. Davies JE. Understanding peri-implant endosseous healing. J Dent Educ 2003;67:932–949.
3. Marco F, Milena F, Gianluca G, Vittoria O. Periimplant osteogenesis in health and osteoporosis. Micron 2005;36: 630–644.
4. Le Gue'hennec L, Soueidan A, Layrolle P, Amouriq Y. Surface treatments of titanium dental implants for rapid osseointegration. Dent Mater 2007;23:844–854.
5. Wennerberg A, Albrektsson T, Albrektsson B, Krol JJ. Histomorphometric and removal torque study of screw-shaped titanium implants with three different surface topographies. Clin Oral Implan Res 1996;6:24–30.
6. Wennerberg A, Hallgren C, Johansson C, Danelli SA. A histomorphometric evaluation of screw-shaped implants each prepared with two surface roughnesses. Clin Oral Implan Res 1998;9:11–19.
7. Cochran DL. A comparison of endosseous dental implant surfaces. J Periodontol 1999;70:1523–1539.
8. Shalabi MM., Gortemaker A, Van't Hof MA, Jansen JA, Creugers NHJ. Implant surface roughness and bone healing: A systematic review. J Dent Res 2006;85:496–500.

9. Mendonça G, Mendonca DBS, Arago FJL, Cooper LF. Advancing dental implant surface technology—From micron- to nanotopography. Biomaterials 2008;29:3822–3835.
10. Park J, Bauer S, Schlegel KA, Neukam FW, Mark KV, Schmuki P. TiO_2 nanotube surfaces: 15 nm—An optimal length scale of surface topography for cell adhesion and differentiation. Small 2009; 5:666–671.
11. McNamara LE, McMurray RJ, Biggs MJP, Kantawong F, Oreffo ROC, Dalby MJ. Nanotopographical control of stem cell differentiation. J Tissue Eng 2010;2010:120623.
12. Puckett S, Pareta R, Webster TJ. Nano rough micron patterned titanium for directing osteoblast morphology and adhesion. Int J Nanomed 2008;3:229–241.
13. Oliveira PT, Nanci A. Nanotexturing of titanium-based surfaces upregulates expression of bone sialoprotein and osteopontin by cultured osteogenic cells. Biomaterials 2004;25:403–413.
14. Subramanian K, Tran D, Nguyen KT. Cellular responses to nanoscale surface modifications of titanium implants for dentistry and bone tissue engineering applications. In: Subramani K, Ahmed W, editors. Emerging Nanotechnologies in Dentistry: Materials, Processes, and Applications. Oxford, UK: Elsevier; 2012. p115–117.
15. Webster TJ, Ejiofor JU. Increased osteoblast adhesion on nanophase metals: Ti, Ti6Al4V, and CoCrMo. Biomaterials 2004;25: 4731–4739.
16. Cooper LF, Zhou Y, Takebe J, Guo J, Abron A, Holmen A, Ellingsen JE. Fluoride modification effects on osteoblast behavior and bone formation at TiO_2 grit-blasted c.p. titanium endosseous implants. Biomaterials 2006;27:926–936.
17. Ellingsen JE, Thomsen P, Lyngstadaas SP. Advances in dental implant materials and tissue regeneration. Periodontol 2000 2006; 41:136–156.
18. Domanski M, Luttge R, Lamers E, Walboomers XF, Winnubst L, Jansen JA, Gardeniers JGE, Submicron-patterning of bulk titanium by nanoimprint lithography and reactive ion etching, Nanotechnology 2012;23:065306.
19. Sul YT, Johansson C, Wennerberg A, Cho LR, Chang BS, Albrektsson T. Optimum surface properties of oxidized implants for reinforcement of osseointegration: Surface chemistry, oxide thickness, porosity, roughness, and crystal structure. Int J Oral Maxillofac Implants 2005;20:349–359.
20. Lee SH, Kim HW, Lee EJ, Li LH, Kim HE. Hydroxyapatite–TiO_2 hybrid coating on Ti implants. J Biomater Appl 2006;20:195–208.
21. Germanier Y, Tosatti S, Broggini N, Textor M, Buser D. Enhanced bone apposition around biofunctionalized sandblasted and acid-etched titanium implant surfaces. A histomorphometric study in miniature pigs. Clin Oral Implants Res 2006;17:251–257.
22. Soler-Illia, GJAA, Sanchez C, Lebeau B, Patarin J. Designed hybrid organic–inorganic nanocomposites from functional nanobuilding blocks. Chem. Rev 2001;13:3061–3083.
23. Ariga K, Hill JP, Lee MV, Vinu A, Charvet R, Acharya S. Challenges and breakthroughs in recent research on self-assembly. Sci Technol Adv Mater 2008;9:014109.
24. Lu Y, Gangull R, Drewlen CA, Anderson MT, Brinker CJ, Gong W, Guo Y, Soyez H, Dunn B, Huang MH, Zink JI. Continuous formation of supported cubic and hexagonal mesoporous films by sol–gel dip-coating. Nature 1997;389:364–368.
25. Brinker CJ, Lu Y, Sellinger A, Fan H. Evaporation-induced self-assembly: nanostructures made easy. Adv Mater 1999;11:579–585.
26. Kuemmel M, Allouche J, Nicole L, Boissièe C, Laberty C, Amenitsch H, Sanchez C, Grosso D. A chemical solution deposition route to nanopatterned inorganic material surfaces. Chem Mater 2007;19:3717–3725.
27. Gomez-Vega JM, Hozumi A, Sugimura H, Takai O. Ordered mesoporous silica coatings that induce apatite formation in vitro. Adv Mater 2001;13:822–825.
28. Biggs MJP, Richards RG, Gadegaard, Wilkinson CDW, Dalby MJ. The effects of nanoscale pits on primary human osteoblast adhesion formation and cellular spreading. J Mater Sci: Mater Med 2007;18:399–404.
29. Cavalcanti-Adam EA, Volberg T, Micoulet A, Kessler H, Geiger B, Spatz JP. Cell spreading and focal adhesion dynamics are regulated by spacing of integrin ligands. Biophys J 2007;92:2964–2974.
30. Dalby MJ, Riehle MO, Johnstone HJH, Affrossman S, Curtis ASG. Nonadhesive nanotopography: Fibroblast response to poly(n-butyl methacrylate)-poly(styrene) demixed surface features. J Biomed Mater Res A 2003;67:1025–1032.
31. Cavalcanti-Adam EA, Micoulet A, Bummel J, Auernheimer J, Kessler H, Spatz JP. Lateral spacing of integrin ligands influences cell spreading and focal adhesion assembly. Eur J Cell Biol 2006; 85:219–224.
32. Dalby MJ, Giannaras D, Riehle MO, Gadegaard N, Affrossman S, Curtis ASG. Rapid fibroblast adhesion to 27 nm high polymer demixed nano-topography. Biomaterials 2004;25:77–83.
33. Sjstrom T, Dalby MJ, Hart A, Tare R, Oreffo ROC, Su B. Fabrication of pillar-like titania nanostructures on titanium and their interactions with human skeletal stem cells. Acta Biomater 2009;5: 1433–1441.
34. Izquierdo-Barba I, Arcos D, Sakamoto Y, Terasaki O, López-Noriega A, Vallet-Regí M. High performance mesoporous bioceramics mimicking bone mineralization. Chem Mater 2008;20:3191–3198.
35. Mabande GTP, Ghosh S, Lai Z, Schwieger W, Tsapatsis M. Preparation of b-oriented MFI films on porous stainless steel substrates. Ind Eng Chem Res 2005;44:9086–9095.
36. Kokubo T, Kushitani H, Sakka S, Kitsugi T, Yamamuro T. Solution able to reproduce in vivo surface-structure change in bioactive glass–ceramic A-W. J Biomed Mater Res 1990;24:723–734.
37. Alberius PCA, Frindell KL, Hayward RC, Kramer WJ, Stucky GD, Chmelka BF. General predictive syntheses of cubic, hexagonal, and lamellar silica and titania mesostructured thin films. Chem Mater 2002;14:3284–3294.
38. Yamada T., Zhou H-S, Uchida H, Tomita M, Ueno Y, Ichino T, Honma I, Asai K. Katsube T. Photovoltage no gas sensor with properties dependent on the structure of the self-ordered mesoporous silicate film. Adv Mater 2002;14:812–815.
39. Miyaji F, Iwai M, Kokubo T, Nakamura T. Effect of heat treatment on apatite-forming ability of Ti metal induced by alkali treatment. J Mater Sci: Mater Med 1998;9:61–65.
40. López-Noriega A, Arcos D, Izquierdo-Barba I, Sakamoto Y, Terasaki, O, M. Vallet-Regí. Ordered mesoporous bioactive glasses for bone tissue regeneration. Chem Mater 2006;18:3137–3144.
41. Kokubo T, Takadama H. How useful is SBF in predicting in vivo bone bioactivity. Biomaterials 2006;27:2907–2915.
42. Rajaraman R, Rounds DE, Yen SPS, Rembaum A. A scanning electron microscope study of cell adhesion and spreading in vitro. Exp Cell Res 1974;88:327–339.
43. Balto H, Al-Nazhan S. Attachment of human periodontal ligament fibroblasts to three different root-end filling materials. Scanning electron microscope observation. Oral Surg 2003;95: 222–227.
44. Anselme K. Osteoblast adhesion on biomaterials. Biomaterials 2000;21:667–681.
45. Hirayama K, Akashi S, Furuya M, Fukuhara K. Rapid confirmation and revision of the primary structure of bovine serum albumin by ESIMS and Frit-FAB LC/MS. Biochem Biophys Res Commun 1990; 173:639–646.
46. Cacciafesta P, Humphries ADL, Jandt KD, Miles MJ. Human plasma fibrinogen adsorption on ultraflat titanium oxide surfaces studied with atomic force microscopy. Langmuir 2000;16: 8167–8175.
47. Covarrubias C, Quijada R. High catalytic activity of SBA-15-supported metallocene toward ethylene polymerization: The effect of the ordered porous structure of the support. Catal Commun 2009; 10:995–1001.
48. Nishimura T, Takeichi M. Remodeling of the adherens junctions during morphogenesis. Curr Top Dev Biol 2009;89:33–54.
49. Boonrungsimana S, Gentlemana E, Carzanigad R, Evansa ND, McComba DW, Portera AE, Stevensa MM. The role of intracellular calcium phosphate in osteoblast-mediated bone apatite formation. PNAS 2012;109:14170–14175.
50. Anderson HC. Matrix vesicles and calcification. Curr Rheumatol Rep 2003;5:222–226.
51. Declercq H, Van den Vreken H, De Maeyer D, Verbeeck R, Schacht E, De Ridder L, Cornelissen M. Isolation, proliferation and differentiation of osteoblastic cells to study cell/biomaterial

interactions: Comparison of different isolation techniques and source. Biomaterials 2004;25:757–768.
52. Guo J, Padilla RJ, Ambrose W, De Kok IJ, Cooper LF. Modification of TiO_2 grit blasted titanium implants by hydrofluoric acid treatment alters adherent osteoblast gene expression in vitro and in vivo. Biomaterials 2007;28:5418–5425.
53. Iza ZM, Schneider GB, Zaharias R, Seabold D. Stanford CM. Effects of fluoride-modified titanium surfaces on osteoblast proliferation and gene expression. Int J Oral Maxillofac Implants 2006; 2:203–211.
54. Guilak F, Cohen DM, Estes BT, Gimble JM, Liedtke W, Chen CS. Control of stem cell fate by physical interactions with the extracellular matrix. Cell Stem Cell 2009;5(1):17–26.
55. Kulangara K, Yang Y, Yang J, Leong KW. Nanotopography as modulator of human mesenchymal stem cell function. Biomaterials 2012;33:4998–5003.
56. Tsigkou O, Jones JR, Polak JM, Stevens MM. Differentiation of fetal osteoblasts and formation of mineralized bone nodules by 45S5 Bioglass conditioned medium in the absence of osteogenic supplements. Biomaterials 2009;21:3542–3550.
57. Bielby RC, Christodoulou IS, Pryce RS, Radford WJ, Hench LL, Polak JM. Time- and concentration-dependent effects of dissolution products of 58S sol–gel bioactive glass on proliferation and differentiation of murine and human osteoblasts. Tissue Eng 2004;10:1018–1026.